ACS Catalysis

Research Article

pubs.acs.org/acscatalysis

Mirroring Enzymes: The Role of Hydrogen Bonding in an Asymmetric Organocatalyzed Aza-Henry Reaction—a DFT Study

Lee Belding, Seyedeh Maryamdokht Taimoory, and Travis Dudding*

Brock University, St. Catharines, Ontario L2S 3A1, Canada

Supporting Information

ABSTRACT: The mechanism of the HQuin-BAM (**1**) catalyzed aza-Henry reaction between nitromethane and *N*-Boc-phenylaldimine was studied using density functional theory (DFT). Deprotonation of nitromethane by the catalyst was revealed to be the rate-limiting step, and C···C bond formation was found to be enantio-determining. The catalyst, in addition to acting as a Brønsted base, served to simultaneously activate both the electrophile and the nucleophile through hydrogen bonding during C···C bond formation and is thus essential for both reaction rate and selectivity. Analysis of the hydrogen bonding interactions revealed that there was a strong preference for the formation of a homonuclear positive-charge-assisted hydrogen bond (homonuclear (+)CAHB), which in turn governed the relative orientation of substrate binding. Furthermore, a direct correlation between the dihedral angle (θ_{NCCN}) of the reacting substrates and facial selectivity was found. This relationship between θ and facial selectivity was found to be a consequence of optimal secondary interactions and orbital overlap.

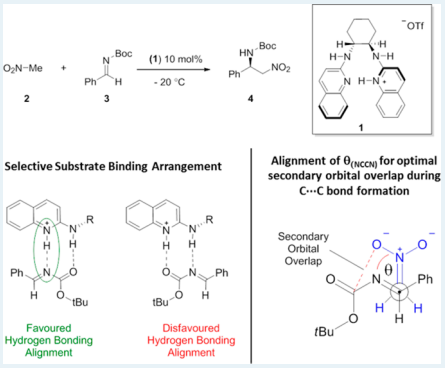

KEYWORDS: *density functional theory, hydrogen bonding, charge assisted hydrogen bond, aza-Henry, asymmetric catalysis, organocatalysis*

INTRODUCTION

Hydrogen bonding[1] is a fundamental element of nature, playing an integral role in nearly all of life's underlying chemical processes. For example, the hydrogen bond is essential in DNA base-pairing, cell-signaling, and enzymatic activity. Specifically, through well-organized hydrogen bonding networks and tailored hydrogen bond activation, enzymes have achieved unparalleled efficiency and specificity[2] rarely equaled by chemists. As a result, the concepts behind enzyme-mediated transformations, in which hydrogen bond activation plays a crucial role, are actively being applied to catalyst design. In this regard, with the aim of mimicking nature's efficiency, catalysts are being developed with substrate-specific cavities, chiral backbones, and multiple activation sites, many of which rely on the use of hydrogen bond motifs.[3] Thus, understanding the spectrum of hydrogen bonding reactivity is essential for continued development in the area of catalytic design, especially for organocatalysts.

Accordingly, the synthesis of chiral organocatalysts with hydrogen bonding sites has attracted substantial attention in recent years,[4] and a number of Brønsted acid subtypes have been implemented in catalyst systems, which are thought to affect hydrogen bond catalysis through distinctly different modes of action.[5] Conventional wisdom asserts that these interactions span a broad range, including bifurcated,[6] σ-bond cooperative (also termed polarization-enhanced or polarization-assisted hydrogen bonding),[7] and π-bond cooperative or resonance-assisted hydrogen bonding.[8]

For instance, it was discovered through an eloquent series of spectroscopic experiments, DFT calculations, and kinetic rate studies that the (*R*,*R*)-1,2-diaminocyclohexane-derived thioureas employed by Jacobson et al. in enantioselective cyanosilylations of ketones,[9] acyl-Pictet Spengler reactions,[10] and Mannich reactions[11] function by means of bifurcated hydrogen bonding. Moreover, this same group in combination with Seidel and others have recently pioneered a conceptually unique approach to asymmetric organocatalysis, wherein chemo-, regio-, and stereoselective induction occurs via the transient formation of a short-lived bifurcated hydrogen bond stabilized anion (i.e., a pseudochiral anion).[12] Furthermore, in 2004, Rawal and co-workers reported a (*R*,*R*)-TADDOL ($\alpha,\alpha,\alpha,\alpha$-tetraaryl-1,3-dioxolane-4,5-dimethanols)-catalyzed enantioselective hetero-Diels–Alder (hDA) reaction of aldehydes with activated dienes and have since reported numerous related organocatalyzed processes.[13] The importance of these findings led to detailed theoretical studies from Domingo as well as Dudding and Houk, which have established that these (*R*,*R*)-TADDOL-catalyzed hDA reactions occur through cooperative H-bond catalysis.[14]

Another important development occurring early on was Johnston et al.'s advancement of a class of chiral bis(amidine) (BAM) Brønsted acid catalysts [e.g., HQuin-BAM (**1**)] for the asymmetric aza-Henry reaction of nitroalkanes (e.g., **2**) and *N*-Boc-phenylaldimines (e.g., **3**) to afford β-nitroamine products (e.g., **4**), which are useful precursors to chiral 1,2-diamines (Scheme 1).[15] A particularly interesting aspect of this organocatalyst was the

Received: July 23, 2014
Revised: November 20, 2014
Published: November 26, 2014

Scheme 1. HQuin-BAM Catalyzed aza-Henry Reaction

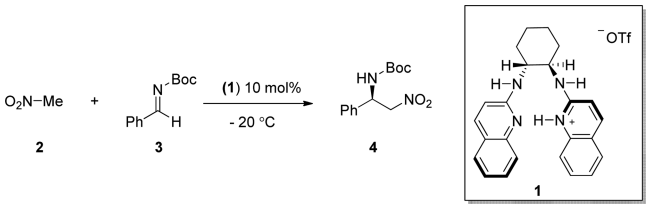

postulated involvement of a polar ionic hydrogen bond. However, at the time, the underlying mechanistic details were poorly understood and remain so even to this day, despite the impressive extension of this work by Johnston.[16] Accordingly, given the continued applications of HQuin-BAM derivatives as catalysts as well as our own interest in how the nature of hydrogen bonding affects asymmetric catalysis, we report herein a detailed mechanistic investigation of the HQuin–BAM-catalyzed aza-Henry reaction pioneered by Johnston and co-workers.

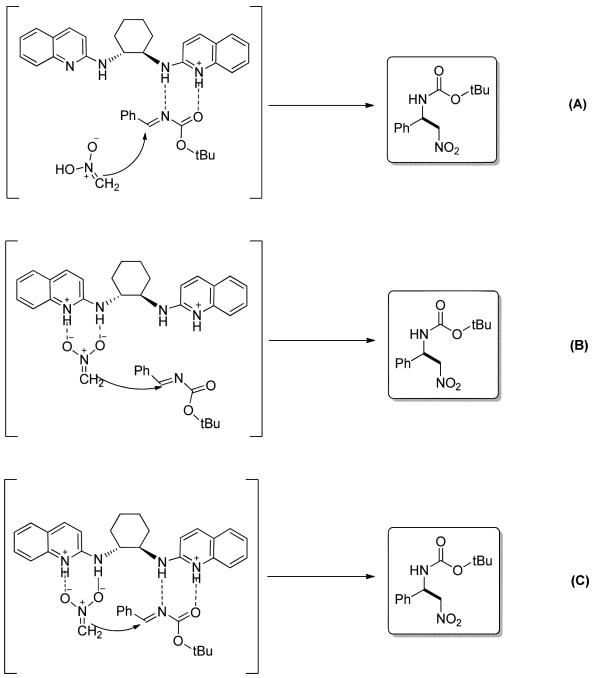

Figure 1. Three possible C···C bond forming events, addition modes A, B, and C.

COMPUTATIONAL METHODOLOGY

All structures were computed using the Gaussian 09[18] suite of programs at the wb97xd[17]/6-31G(d) level of theory, implementing the integrated equation formalism polarized continuum solvation model (IEFPCM)[19] to account for solvent effects (default solvent parameters for nitromethane were used). All minima were confirmed by the presence of only real vibrational frequencies, and transition states were confirmed to have one imaginary frequency. Thermochemical quantities were evaluated at 253 K, and the IRC methodology was used to obtain the minima on either side of each transition state. Natural bond orbital analysis (NBO Version 3.1 as implemented in Gaussian 09) was used to quantify the electronic donor–acceptor interactions as second-order perturbation energies (E_{NBO}). For simplicity, the triflate counterion was omitted from the calculations.

RESULTS AND DISCUSSION

At the outset of this study, working under the assumption that C···C bond formation between *N*-Boc-phenylaldimine and either an in situ-derived nitroenolate (i.e., nitronate) or nitroenol species was stereodetermining, three possible mechanistic scenarios were investigated: namely, addition modes A, B, and C (Figure 1). Addition mode A corresponds to nucleophilic attack of nitroenol to a catalyst-bound *N*-Boc-phenylaldimine, whereas in addition mode B, a catalyst activated nitronate adds to an unactivated *N*-Boc-phenylaldimine. Last, addition mode C involves activation of both the nitronate nucleophile and the *N*-Boc-phenylaldimine electrophile during C···C bond formation.

When initially considering this catalytic system, two key functions were identified: hydrogen bond (H-bond) activation and chiral induction. To properly understand the nature of the first of these variables (H-bond activation), it was important that it be investigated in the absence of the chiral environment. To achieve this, we examined the effect of achiral catalyst 2-(methylamino)pyridine-1-ium on the reaction between nitromethane and a truncated aldimine, *N*-methyl methylenecarbamate (see Figure 2).

Emerging from the computed addition mode A were two potential binding orientations between the aldimine and the catalyst (**TS-A1** and **TS-A2**, Figure 2). In both orientations, the lowest energy transition states possessed C···C bond forming distances of 2.0 Å and a synclinal arrangement with respect to the approaching nucleophile (N–C–C–N dihedral angle, θ = 34° for **TS-A1** and θ = 31° for **TS-A2**). Considering these similarities, it stands to reason that the 0.8 kcal/mol energetic preference for

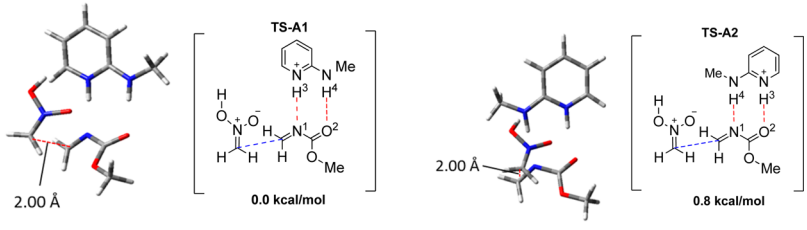

TS-A1	Bond Distance (Å)	ΔE_{NBO} (kcal/mol)	TS-A2	Bond Distance (Å)	ΔE_{NBO} (kcal/mol)
$N^1\cdots(N^+)H^3$	1.75	43.8	$N^1\cdots(N)H^4$	1.87	29.3
$O^2\cdots(N)H^4$	1.86	14.4	$O^2\cdots(N^+)H^3$	2.76	21.0

Figure 2. wb97xd/6-31G(d) Calculated C···C bond forming transition states (**TS-A1** and **TS-A2**) for addition mode A.

dx.doi.org/10.1021/cs501062u | *ACS Catal.* 2015, 5, 343–349

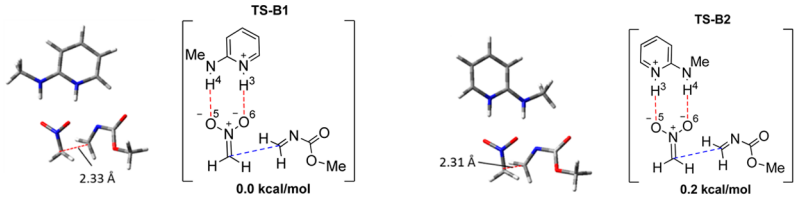

TS-B1	Bond Distance (Å)	ΔE_{NBO} (kcal/mol)	TS-B2	Bond Distance (Å)	ΔE_{NBO} (kcal/mol)
$O^5\cdots(N)H^4$	1.79	13.7	$O^5\cdots(N)H^4$	1.65	4.7
$O^6\cdots(N^+)H^3$	1.80	25.6	$O^6\cdots(N^+)H^3$	2.10	44.4

Figure 3. wb97xd/6-31G(d) Calculated C···C bond forming transition states (**TS-B1** and **TS-B2**) for addition mode B.

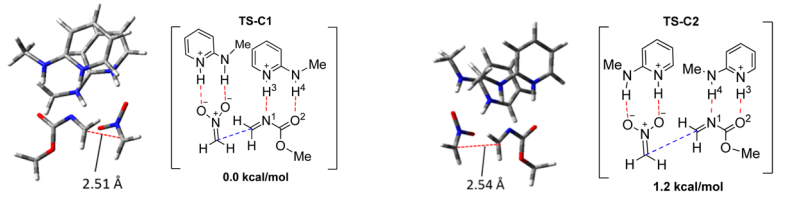

TS-C1	Bond Distance (Å)	ΔE_{NBO} (kcal/mol)	TS-C2	Bond Distance (Å)	ΔE_{NBO} (kcal/mol)
$N^1\cdots(N^+)H^3$	1.78	38.5	$N^1\cdots(N)H^4$	1.90	25.6
$O^2\cdots(N)H^4$	1.89	14.3	$O^2\cdots(N^+)H^3$	1.80	20.6

Figure 4. wb97xd/6-31G(d) Calculated C···C bond forming transition states (**TS-C1** and **TS-C2**) for addition mode C.

TS-A1 over **TS-A2** is solely a result of the difference in hydrogen bonding interactions between the two transition states. Accordingly, to better understand these hydrogen bonding interactions, we turned to natural bond orbital (NBO) analysis, which revealed that the homonuclear H-bonds (in which the donor and acceptor atoms are the same) in both structures are stronger than the heteronuclear H-bonds (in which the donor and acceptor atoms are different), presumably as a result of better pK_a matching.[20] Moreover, it was found that the homonuclear positive charge assisted hydrogen bond (homonuclear (+)CAHB, i.e., $N^+{-}H^3\cdots N^1$) present in **TS-A1** displayed a significantly stronger stabilization energy (E_{NBO} = 43.8 kcal/mol) than that of the neutral homonuclear H-bond present in **TS-A2** (E_{NBO} = 29.3 kcal/mol), thus suggesting that the preferred binding alignment is a consequence of maximizing the strength of the positive charged assisted hydrogen bond.

Alternatively, addition mode B involves nucleophilic addition of a H-bond stabilized nitronate to a free electrophile (Figure 3); however, this time, because of the absence of hydrogen bonding to the electrophile, the two comparative substrate orientations (analogous to those in addition mode A) were nearly isoenergetic ($\Delta G^{\ddagger}$ = 0.2 kcal/mol). In both **TS-B1** and **TS-B2**, the C···C bond-forming distances (2.33 and 2.31 Å) were slightly elongated when compared with **TS-A1** and **TS-A2**, whereas θ retained a similar synclinal alignment of 39.4° and 38.1°. Notably, the uncatalyzed addition of nitronate to aldimine (**TS-D1**, **TS-D2**; Supporting Information), was found to be energetically disfavored with respect to addition mode A and B (see Supporting Information Table S1 for the relative energies of each addition mode), suggesting that the catalyst imparts a degree of stabilization to the C···C bond-forming transition state when bound to either the nucleophile or the electrophile.

Finally, addition mode C, which is effectively a composite of addition modes A and B, involving catalyst activation of the aldimine electrophile and stabilization of the nucleophilic nitronate (Figure 4), was found to be significantly favored (see Table S1, Supporting Information). Analogous to addition mode A, in addition mode C, the preferential hydrogen bonding framework is that with the strongest homonuclear (+)CAHB ($N^+{-}H^3\cdots N^1$); however, the presence of a second catalyst fragment forces the substrates into a nearly synperiplanar arrangement (**TS-C1** $\theta_{(N-C-C-N)}$ = 14° and **TS-C2** $\theta_{(N-C-C-N)}$ = −15°) to alleviate steric strain. Although a synclinal arrangement is preferred, as seen in addition modes A and B (vida infra), this factor is apparently outweighed by simultaneous activation of both reacting components. Thus, the H-bond stabilization of both reaction components reduces the activation energy required for C···C bond formation insofar as to supersede otherwise unfavorable structural and electronic factors. Therefore, one can conclude from the truncated models that the activation barrier to C···C bond formation is reduced upon either activation of the electrophile or stabilization of the nucleophile, with dual activation/stabilization being preferred. Furthermore, it was found that the formation of a homonuclear (+)CAHB dictated the preferred alignment between the aldimine and the catalyst. Thus, it can be said that the catalyst acts in a manner similar to an enzyme, wherein subtle pK_a differences in the hydrogen bond donors guide the substrates into proper binding alignment for optimal transition state stabilization.

At that stage, having investigated the influence of hydrogen bonding in this catalytic system through a series of truncated models, the role of the chiral diamine motif in **1** on enantioselective C···C bond formation was investigated. Consistent with the truncated models, transition states for nitronate addition to

dx.doi.org/10.1021/cs501062u | ACS Catal. 2015, 5, 343−349

N-Boc-phenylaldimine computed in the presence of **1** were found to be significantly favored when both substrates were bound to the catalyst, reminiscent of pathway C (see Supporting Information Table S2 for a comparison of relative transition state energies). Likewise, homonuclear (+)CAHB (N^+-H^3···N^1), such as that present in the truncated models, was found in both the lowest energy pro-(*R*) and pro-(*S*) transition states (**pro-(*R*)-TS1** and **pro-(*S*)-TS1**, respectively, Figure 5), thus supporting the preference for this underlying hydrogen bonding framework, even in the presence of the chiral backbone. Given the analogous hydrogen bonding framework in both **pro-(*R*)-TS1** and **pro-(*S*)-TS1**, a more rigorous inspection of these two transition states was carried out to gain insight into the factors contributing to asymmetric induction.

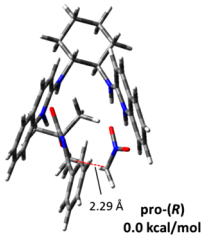

pro-(*R*)-TS1	Bond Distance (Å)	ΔE_{NBO} (kcal/mol)
N^1•••$(N^+)H^{3a}$	1.82	31.2
O^2•••$(N)H^{4a}$	1.71	26.9
O^5•••$(N)H^{3b}$	1.76	24.7
O^6•••$(N^+)H^{4b}$	1.63	41.3

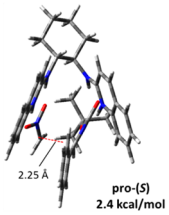

pro-(*S*)-TS1	Bond Distance (Å)	ΔE_{NBO} (kcal/mol)
N^1•••$(N^+)H^{3a}$	1.74	36.3
O^2•••$(N)H^{4a}$	1.84	11.0
O^5•••$(N)H^{4b}$	1.85	16.4
O^6•••$(N^+)H^{4b}$	1.66	30.5

Figure 5. wb97xd/6-31G(d) Calculated C···C bond forming transition states (**pro-(*R*)-TS1** and **pro-(*S*)-TS1**) for addition mode C.

Consistent with the experimental results of Johnston, the pro-(*R*) transition state energy was 2.4 kcal/mol lower in than that of the pro-(*S*) transition state (corresponding to 98% ee), with activation barriers of 3.5 and 5.9 kcal/mol, respectively. Although the computations overestimate the 60% ee observed experimentally by Johnston, it should be noted that the estimation improves with higher levels of theory (see Supporting Information Table S3). To this end, a distortion/interaction analysis (Figure 6, eqs 1−3) was carried out to discern the rather subtle structural differences which accounted for the 2.4 kcal/mol energetic difference between **pro-(*R*)-TS1** and **pro-(*S*)-TS1**.

The distortion/interaction analysis for the case at hand is broken down as follows: eq 1 describes the interaction energy between the catalyst and the two substrates in their transition state geometry, where **I** represents the full transition state assembly, **II** represents the catalyst in its transition state geometry, and **III** corresponds to the reacting substrates unperturbed from their transition state geometry. Equation 2 describes the distortion within the catalyst backbone at the transition state, compared with its ground state. Meanwhile, eq 3 represents the distortion/interaction energy between the two reacting component at the transition state (**III**), relative to their ground states (**IV** and **V**).

The interaction energy (eq 1) was expectedly large for both **pro-(*R*)-TS1** and **pro-(*S*)-TS1** (E_{int} = 51.8 and 51.5 kcal/mol, respectively); however, the energy difference between the two

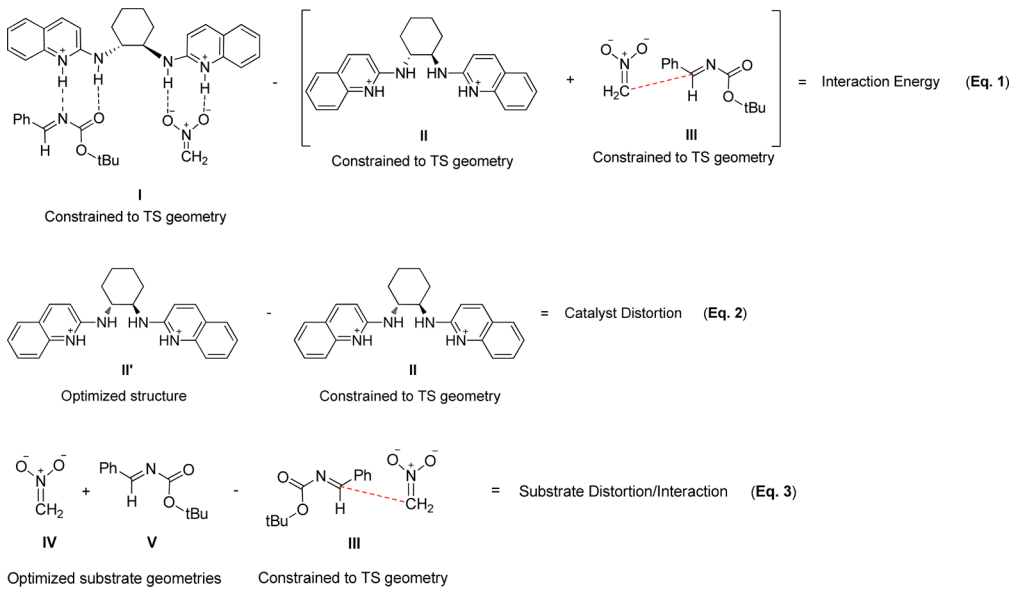

Figure 6. Distortion/interaction analysis (eqs 1−3) for the wb97xd/6-31G(d) calculated C···C bond forming transition states (**pro-(*R*)-TS1** and **pro-(*S*)-TS1**).

dx.doi.org/10.1021/cs501062u | *ACS Catal.* 2015, 5, 343−349

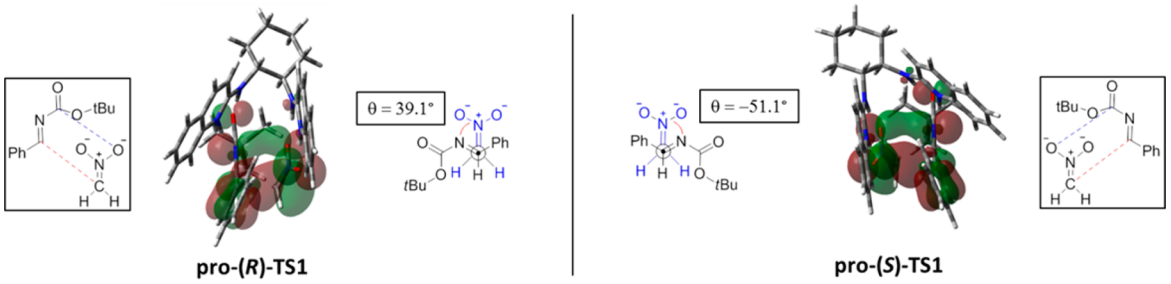

Figure 7. Depiction of the substrate alignment and secondary interactions and orbital overlap within the wb97xd/6-31G(d) calculated C···C bond forming transition states **pro-(*R*)-TS1** and **pro-(*S*)-TS1**. 3D models represent the HOMO for each transition state.

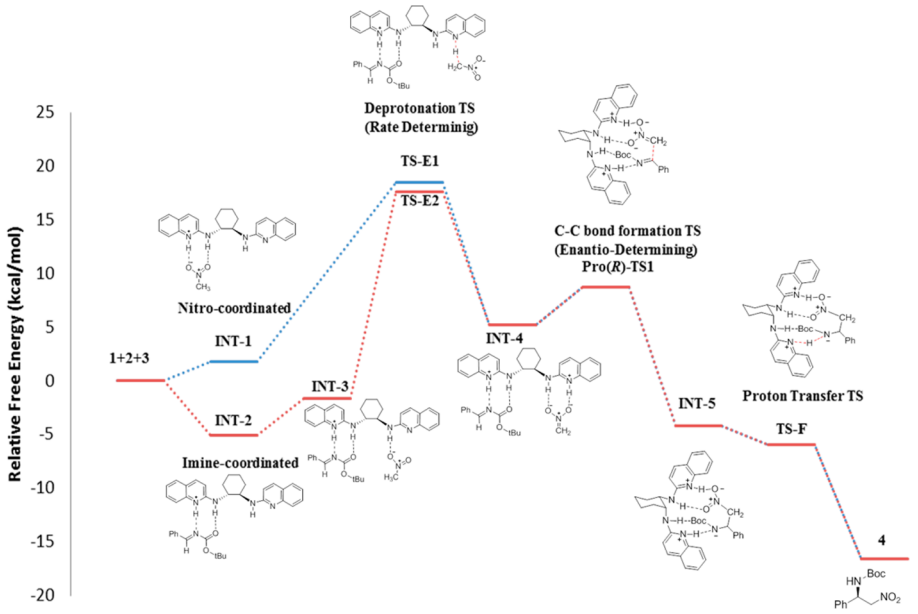

Figure 8. wb97xd/6-31G(d) calculated free energy diagram of the HQuin-BAM catalyzed enantioselective aza-Henry reaction.

addition modes was minimal (ΔE_{int} = 0.3 kcal/mol), likely as a result of the analogous hydrogen bonding network. On the other hand, the effect of catalyst distortion (eq 2) was small relative to that of the interaction energy (E_{dist} = 9.2 and 9.8 kcal/mol), although it contributed slightly more to the energetic preference for the pro-(*R*) stereofacial mode of addition (ΔE_{dist} = 0.6 kcal/mol). Finally, the substrate distortion/interaction (eq 3) had the smallest absolute energetic contribution ($E_{dist/int}$ = 4.9 and 4.0 kcal/mol) but the largest influence on the energetic discrepancy between the two stereofacial addition modes ($\Delta E_{dist/int}$ = 0.9 kcal/mol) and was thus taken as the dominant factor contributing to facial selectivity. Following from this, a comparison of the two stereofacial addition modes, $\mathbf{III}_{pro(S)}$ and $\mathbf{III}_{pro(R)}$, revealed that a substantial difference in attack orientation existed between the two stereofacial addition modes (previously defined by the dihedral angle θ). Placed in the context of addition modes A and B, the truncated models freed of all steric and structural artifacts linked to the catalyst backbone, the ideal substrate alignment is synclinal, with an angle of θ = 30−40°; thus, one might expect the attainment of such an angle to be optimal. Consistent with this reasoning, in the favored transition state, **pro-(*R*)-TS1**, the nitronate and *N*-Boc phenylaldimine share a synclinal attack orientation $\theta_{pro(R)}$ = 39.1°, whereas in **pro-(*S*)-TS1**, they approach one another at an angle $\theta_{pro(S)}$ = −51.1°. The origin of this preferential attack trajectory was traced to the observed secondary orbital overlap between the two reacting components at the transition state, as seen from the HOMOs in Figure 7. A subsequent NBO analysis revealed that a synclinal attack alignment allows for the optimization of secondary interactions between the nitronate oxygen atom and the antibonding orbital of carbonyl group in *N*-Boc-phenylaldimine (Figure 7; **pro-(*R*)-TS1**, $E_{(NBO)}$ = 2.6; **pro-(*S*)-TS1**, $E_{(NBO)}$ = 0.6 kcal/mol). Taken together, the specific substrate binding mode governed by the asymmetric hydrogen bonding framework of the chiral catalyst, along with subtle secondary orbital interactions, leads to the observed stereochemical induction, and in reflection, it would appear that many parallels can be drawn between the function of this organocatalyst and that of an enzyme.

Having determined the origin of stereoinduction, we next turned to the reaction mechanism as a whole (Figure 8, see the Supporting Information for structural details). The reaction pathway begins with coordination of *N*-Boc-phenylaldimine to the catalyst (**INT-2**), followed by docking of nitromethane (**INT-3**), which undergoes subsequent catalyst facilitated deprotonation.

Alternatively, a reaction scenario involving coordination of free nitroenol to afford **INT-4** is doubtful, given the exceptionally low equilibrium constant between nitromethane and nitroenol (1.1×10^{-7}) at room temperature.[21] As such, it is likely that the catalyst serves as a base to deprotonate nitromethane, and two competing deprotonation transition states were located (**TS-E1** and **TS-E2**, Figure 9).

dx.doi.org/10.1021/cs501062u | *ACS Catal.* 2015, 5, 343−349

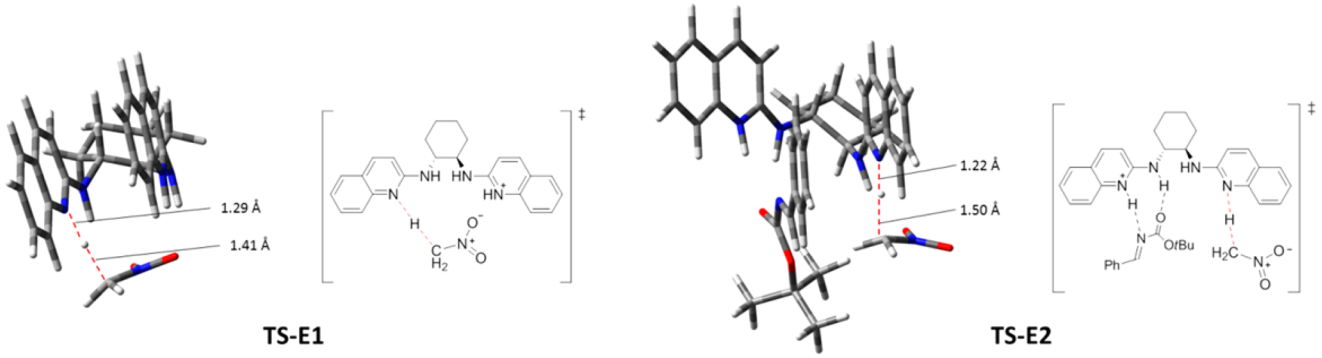

Figure 9. wb97xd/6-31G(d) Calculated deprotonation transition states (**TS-E1** and **TS-E2**).

The favored deprotonation transition state, **TS-E2**, possesses a N···H bond-forming distance of 1.22 Å and a C···H bond-breaking distance of 1.50 Å. Interestingly, the preferred transition state is that in which *N*-Boc-phenylaldimine is already coordinated to the protonated half of the catalyst, as opposed to deprotonation via a free catalyst (**TS-E1**). The preference of **TS-E2** over **TS-E1** ($\Delta G^{\ddagger}$ = 0.9 kcal/mol) follows nicely from the fact that coordination of *N*-Boc-phenylaldimine to the catalyst (intermediate **INT-2**) is energetically favored over coordination of nitromethane (intermediate **INT-1**). Regardless, deprotonation of nitromethane is calculated to be rate-limiting. At that stage, a subtle shift in the nitronate alignment results in **INT-4**, in which the catalyst-bound substrates are in close proximity and in proper alignment for enantiodetermining C···C bond formation, **pro-(*R*)-TS1.** The ensuing charged separated intermediate (**INT-5**) then undergoes proton transfer (**TS-F**), resulting in product formation and catalyst regeneration.

CONCLUSIONS

In conclusion, the mechanism of the HQuin-BAM (**1**) catalyzed aza-Henry reaction between nitromethane and *N*-Boc-phenylaldimine was studied using density functional theory. Deprotonation of nitromethane by the catalyst was revealed to be the rate-limiting step, and C···C bond formation was found to be enantio-determining. The catalyst, in addition to acting as a Brønsted base to generate a nitroenolate, served subsequently as a Brønsted acid to simultaneously activate the electrophile and stabilize the nucleophile through hydrogen bonding during C···C bond formation and is thus essential for both reaction rate and selectivity. Analysis of the hydrogen bonding interactions revealed that there was a strong preference for the formation of homonuclear (+)CAHB, which in turn governed the relative orientation of substrate binding. Furthermore, a direct correlation was observed between the dihedral angle (θ_{NCCN}) of the reacting substrates and facial selectivity. This relationship was found to be a consequence of optimal secondary interactions and orbital overlap. Taken together, mechanistically, the catalyst imposes a specific substrate binding alignment, plays multiple roles in the transformation, and imparts a chiral environment, thus strongly resembling the actions of an enzyme. The insight gained into the effect of different hydrogen bonding modes on the preferred binding arrangement should facilitate future advancements in H-bond based organocatalysis. A priori knowledge of substrate binding alignment to a given catalyst will facilitate computationally based catalyst screening as well as the rational design of future catalysts.

ASSOCIATED CONTENT

Supporting Information

The following file is available free of charge on the ACS Publications website at DOI: 10.1021/cs501062u.

Coordinate and thermochemical data for all structures, including the computed transition state structures for the uncatalyzed pathway (**TS-D1**, **TS-D2**), the computed transition states in the presence of the asymmetric HQuin–BAM catalyst (**TS-A3**, **TS-A4**, **TS-B3**, **TS-B4**, **TS-C3**, **TS-C4**), and the optimized structures of the related precomplexes and products (PDF)

AUTHOR INFORMATION

Corresponding Author

*E-mail: tdudding@brocku.ca.

Notes

The authors declare no competing financial interest.

ACKNOWLEDGMENTS

The authors would like to thank Sharcnet for computing resources. Financial support was provided in part by NSERC. L.B. is grateful for a QEII scholarship and an NSERC CGS scholarship, and S.M.T. thanks Thrillium Ontario Scholarship for financial support.

REFERENCES

(1) (a) Pimentel, G. C.; McClellan, A. L *The Hydrogen Bond*; Freeman: San Francisco, 1960. (b) Jeffrey, G. A. *An Introduction to Hydrogen Bonding*; Oxford University: New York, 1997. (c) Scheiner, S. *Hydrogen Bonding. A Theoretical Perspective*; Oxford University Press: Oxford, 1997. (d) Steiner, T. *Angew. Chem., Int. Ed.* **2002**, *41*, 48–76. (e) Weinhold, F.; Klein, R. A. *Mol. Phys.* **2012**, *110*, 565–579.

(2) (a) Jeffrey, G.; Saenger, W. *Hydrogen Bonding in Biological Structures*; Springer: Berlin, 1991. (b) Desiraju, G. R.; Steiner, T. *The Weak Hydrogen Bond in Structural Chemistry and Biology*; Oxford University Press: Oxford, 1999. (c) Schowen, K. B.; Limbach, H.-H.; Denisov, G. S.; Schowen, R. L. *Biochim. Biophys. Acta* **2000**, *1458*, 43–62. (d) Silverman, R. B. *The Organic Chemistry of Enzyme Catalyzed Reactions*; Academic: San Diego, CA, 2002.

(3) (a) Pihko, P. M. *Angew. Chem.* **2004**, *43*, 2026–2064. (b) Schreiner, P. R. *Chem. Soc. Rev.* **2003**, *32*, 289–296. (c) Taylor, M. S.; Jacobsen, E. N. *Angew. Chem., Int. Ed.* **2006**, *45*, 1520–1543.

(4) (a) Doyle, A. G.; Jacobsen, E. N. *Chem. Rev.* **2007**, *107*, 5713–5743. (b) Yu, X.; Wang, W. *Chem.—Asian J.* **2008**, *3*, 516–532. (c) Liu, X.; Lin, L.; Feng, X. *Chem. Commun.* **2009**, 6145–6158. (d) Ha-Yeon Cheong, P.; Legault, C. Y.; Um, J. M.; Celebi-Olcum, N.; Houk, K. N. *Chem. Rev.* **2011**, *111*, 5042–5137.

(5) (a) Rozas, I.; Alkorta, I.; Elguero, J. *J. Phys. Chem. A* **1998**, *102*, 9925–9932. (b) Gilli, G.; Gilli, P. *J. Mol. Struct.* **2000**, *552*, 1–15.

(c) Gilli, P.; Pretto, L.; Bertolasi, V.; Gilli, G. *Acc. Chem. Res.* **2009**, *42*, 33−44.
(6) Rozas, I.; Alkorta, I.; Elguero, J. *J. Phys. Chem. A* **1998**, *102*, 9925−9932.
(7) (a) Jeffrey, G. A. *An Introduction to Hydrogen Bonding*; Oxford University Press: Oxford, 1997. (b) Jeffrey, G. A. *Crystallogr. Rev.* **1995**, *3*, 213−260.
(8) (a) Gilli, G.; Bellucci, F.; Ferretti, V.; Bertolasi, V. *J. Am. Chem. Soc.* **1989**, *111*, 1023−1028. (b) Bertolasi, V.; Gilli, P.; Ferretti, V.; Gilli, G. *J. Am. Chem. Soc.* **1991**, *113*, 4917−4925.
(9) Fuerst, D. E.; Jacobsen, E. N. *J. Am. Chem. Soc.* **2005**, *127*, 8964−896.
(10) Taylor, M. S.; Jacobsen, E. N. *J. Am. Chem. Soc.* **2004**, *126*, 10558−10559.
(11) Yoon, T. P.; Jacobsen, E. N. *Angew. Chem., Int. Ed.* **2005**, *44*, 466−468.
(12) (a) De, C. K.; Seidel, D. *J. Am. Chem. Soc.* **2011**, *133*, 14538−14541. (b) Knowles, R. R.; Lin, S.; Jacobsen, E. N. *J. Am. Chem. Soc.* **2010**, *132*, 5030−5032. (d) Peterson, E. A.; Jacobsen, E. N. *Angew. Chem., Int. Ed.* **2009**, *48*, 6328−6331. (e) Brown, A. R.; Kuo, W.; Jacobsen, E. N. *J. Am. Chem. Soc.* **2010**, *132*, 9286−9288.
(13) Thadani, A. N.; Stankovic, A. R.; Rawal, V. H. *PNAS.* **2004**, *101*, 5846−5850.
(14) (a) Gordillo, R.; Dudding, T.; Anderson, C. D.; Houk, K. N. *Org. Lett.* **2007**, *9*, 501−503. (b) Anderson, C. D.; Dudding, T.; Gordillo, R.; Houk, K. N. *Org. Lett.* **2008**, *10*, 2749−2752. (c) Domingo, L. R.; Andres, J. *J. Org. Chem.* **2003**, *68*, 8662−8668. (d) Polo, V.; Domingo, L. R.; Andres, J. *J. Phys. Chem. A* **2005**, *109*, 10438−10444.
(15) Nugent, B. M.; Yoder, R. A.; Johnston, J. N. *J. Am. Chem. Soc.* **2004**, *126*, 3418−3419.
(16) (a) Hess, A. S.; Yoder, R. A.; Johnston, J. N. *Synlett* **2006**, *1*, 147−149. (b) Dobish, M. C.; Johnston, J. N. *Org. Lett.* **2010**, *12*, 5744−5747. (c) Davis, T. A.; Wilt, J. C.; Johnston, J. M. *J. Am. Chem. Soc.* **2010**, *132*, 2880−2882. (d) Shen, B.; Makley, D. M.; Johnston, J. N. *Nature* **2010**, *465*, 1027−1033. (e) Davis, T. A.; Johnston, J. N. *Chem. Sci.* **2011**, *2*, 1076. (f) Davis, T. A.; Danneman, M. W.; Johnston, J. N. *Chem. Commun.* **2012**, *48*, 5578−5580. (g) Dobish, M. C.; Johnston, J. N. *J. Am. Chem. Soc.* **2012**, *134*, 6068−6071. (h) Davis, T. A.; Vilgelm, A. E.; Richmond, A.; Johnston, J. N. *J. Org. Chem.* **2013**, *78*, 10605−10616. (i) Vara, B. A.; Mayasundari, A.; Tellis, J. C.; Danneman, M. W.; Arredondo, V.; Davis, T. A.; Min, J.; Finch, K.; Guy, R. K.; Johnston, J. N. *J. Org. Chem.* **2014**, *79*, 6913−6938.
(17) Chai, J.-D.; Head-Gordon, M. *Phys. Chem. Chem. Phys.* **2008**, *10*, 6615−6620.
(18) Frisch, M. J.; Trucks, G. W.; Schlegel, H. B.; Scuseria, G. E.; Robb, M. A.; Cheeseman, J. R.; Scalmani, G.; Barone, V.; Mennucci, B.; Petersson, G. A.; Nakatsuji, H.; Caricato, M.; Li, X.; Hratchian, H. P.; Izmaylov, A. F.; Bloino, J.; Zhang, G.; Sonnenberg, J. L.; Hada, M.; Ehara, M.; Toyota, K.; Fukuda, R.; Hasegawa, J.; Ishida, M.; Nakajima, T.; Honda, Y.; Kitao, O.; Nakai, H.; Vreven, T.; Montgomery, J. A.; Peralta, Jr., J. E.; Ogliaro, F.; Bearpark, M.; Heyd, J. J.; Brothers, E.; Kudin, K. N.; Staroverov, V. N.; Kobayashi, R.; Normand, J.; Raghavachari, K.; Rendell, A.; Burant, J. C.; Iyengar, S. S.; Tomasi, J.; Cossi, M.; Rega, N.; Millam, J. M.; Klene, M.; Knox, J.e.; Cross, J. B.; Bakken, V.; Adamo, C.; Jaramillo, J.; Gomperts, R.; Stratmann, R. E.; Yazyev, O.; Austin, A. J.; Cammi, A. R.; Pomelli, C.; Ochterski, J. W.; Martin, R. L.; Morokuma, K.; Zakrzewski, V. G.; Voth, G. A.; Salvador, P.; Dannenberg, J. J.; Dapprich, S.; Daniels, A. D.; Farkas, Ö.; Foresman, J. B.; Ortiz, J. V.; Cioslowski, J.; Fox, D. J.*Gaussian 09, Revision C.02*; Gaussian, Inc.: Wallingford, CT, 2009.
(19) Tomasi, J.; Mennucci, B.; Cance, E. *J. Mol. Struct.* **1999**, *464*, 211−226.
(20) Gilli, P.; Pretto, L.; Gilli, G. *J. Mol. Struct.* **2007**, *844*−*845*, 328−339.
(21) (a) Lammertsma, K.; Prasad, B. V. *J. Am. Chem. Soc.* **1993**, *115*, 2348−2351. (b) Turnbull, D.; Maron, S. H. *J. Am. Chem. Soc.* **1943**, *65*, 212−218.